第 50 卷 第 18 期/2023 年 9 月/中国激光 研究论文

中国激光

路径导引的四波横向剪切干涉波前重构方法

闵星植[1,2,3]，段亚轩[1,3*]，王拯洲[1,3]，陈晓义[1,3]，唐志愿[1,3]，王璞[1,3]，范尧[1,3]

[1]中国科学院西安光学精密机械研究所先进光学仪器研究室，陕西 西安 710119；

[2]中国科学院大学，北京 100049；

[3]西安市高功率激光测量技术与仪器重点实验室，陕西 西安 710119

摘要 为了解决区域法在四波横向剪切干涉波前重构过程中噪声误差沿积分路径累积影响波前重构精度的问题，本文提出了一种路径导引的四波横向剪切干涉波前重构方法。首先分析了噪声环境下无积分路径导引的区域法波前重构存在噪声误差累积的缺陷，然后在此基础上建立了基于差分相位导数偏差的积分路径评价图模型，并给出了基于积分路径导引的波前重构算法流程。为了验证所提方法的有效性，本文进行了理论仿真研究，结果表明在不同信噪比噪声下所提方法能有效地阻止噪声误差的传播和累积。搭建了基于纯相位型液晶空间光调制器的实验验证装置，实验结果表明：所提方法重构波前与理论波前残差的RMS相比无积分路径导引区域法重构波前与理论波前残差的RMS降低了39.7%，且所提方法重构波前PV值与理论波前PV值的偏差相对无积分路径导引区域法重构波前PV值与理论波前PV值的偏差减小了1.6943λ。所提方法可为提高噪声环境下四波横向剪切干涉波前重构精度提供一种有效方法。

关键词 测量；波前重构；路径导引；四波横向剪切干涉；差分相位

中图分类号 O436 **文献标志码** A **DOI**：10.3788/CJL221344

1 引 言

随着数字社会的快速发展，航空航天、电子、军事等领域对光学系统提出了更高要求。光学干涉仪为光学元件和系统的评价、检测提供了一种复杂且有效的方法。四波横向剪切干涉仪(QWLSI)利用改进的哈特曼模板(MHM)[1-2]作为分光元件，通过单幅干涉图同时采集两个正交方向上的剪切波前数据来进行瞬态相位测量。QWLSI具有系统紧凑和共光路的特点，且不易受环境的影响，因此被广泛应用于极紫外波前计量[3]、系统像差测量[4-5]和活体细胞定量相位成像[6-12]等领域。

通过对QWLSI采集到的干涉图进行解调、滤波、相位解包裹等处理，可以获得剪切方向上的差分相位，进而通过波前重构方法可以重构出待测波前。QWLSI的波前重构方法通常可以分为模式法和区域法，这两类方法已被国内外广泛研究。利用模式法重构波前[2,13-23]时，波前被扩展为一组基函数，这组基函数对应的系数由不同的波前拟合得到(通常将Zernike多项式作为波前扩展的基函数[14-22])。目前有4种典型的基于Zernike多项式的模态重建方法，分别是Rimmer-Wyan方法[3]、椭圆正交变换法[3]、数值正交变换法[16]和差分Zernike多项式拟合法[17]。这些方法的重构误差不仅来自波前的测量噪声，还来自被忽略的剩余高阶项[3,9]。利用区域法重构波前[20-30]时，先将待测波前离散化，建立待测波前与差分波前每个像素之间的点对点映射关系，再进行求解，或者沿剪切方向进行积分，重构出待测波前。传统的区域法重构模型包括Hudgin模型[24]、Fried模型[25]和Southwell模型[26]，其中Southwell模型的测量点与重构波前相位点位于同一位置，且每个重构波前相位点都包含x和y方向的差分相位测量值，具有更高的重构精度[24]，所以通常采用Southwell作为区域法波前重构模型。相比模式法，区域法具有更高的空间分辨率[29]，但在重构过程中，区域法存在最优积分路径选择问题，若不按照最优路径重构积分，噪声就会沿积分方向传播、累积，降低波前重构精度。

为解决区域法存在的噪声沿积分路径传播、累积的问题，笔者提出了一种以差分相位导数偏差评价图为模型的四波横向剪切干涉波前重构方法。该方法首先利用差分相位获取一幅带有积分路径导引的评价图，然后根据该积分路径进行波前重构积分，即可阻止噪声沿积分路径的叠加与传播，提高波前重构精度。

收稿日期：2022-10-19；**修回日期**：2022-12-03；**录用日期**：2022-12-16；**网络首发日期**：2022-12-26

基金项目：国家自然科学基金(61705254)、国家重点研发计划(2021YFC2203501)、陕西省重点研发计划(2020GY-114)

通信作者：*duanyaxuan@opt.ac.cn

2 理　论

2.1 区域法波前重构

区域法是在已知差分波前的情况下，通过求解纽曼边界条件下的泊松方程得到待测波前的方法。其求解方法分为两种：一种是通过建立待测相位与差分相位之间的矩阵关系[31]进行求解，其求解难点为系数矩阵不可逆[31]，处理过程相对复杂；另一种是沿着路径对差分相位进行数值积分[1,31]，即

$$\varphi(r)=\int_{C}\nabla\varphi\cdot\mathrm{d}r+\varphi(r_0),\tag{1}$$

式中，C是积分区域（重构区域）内的一条连接r_0到r的任意积分路径，$\nabla\varphi$是待测相位$\varphi(r)$的梯度，r_0为积分起始点，$\mathrm{d}r=\mathrm{d}x+\mathrm{d}y$，$\varphi(r_0)=\varphi(x_0,y_0)$。因为

$$\nabla\varphi=\frac{\partial\varphi}{\partial x}+\frac{\partial\varphi}{\partial y},\tag{2}$$

所以待测相位可以改写成

$$\varphi(x,y)=\int_{C}\left(\frac{\partial\varphi}{\partial x}\mathrm{d}x+\frac{\partial\varphi}{\partial y}\mathrm{d}y\right)+\varphi(x_0,y_0)。\tag{3}$$

离散化处理后，根据测量的波前相位差分点与重构波前相位点的位置差异，采用Southwell模型进行波前重构。Southwell模型进行波前重构的原理如图1所示。被测差分相位与重构相位的关系可以表示为

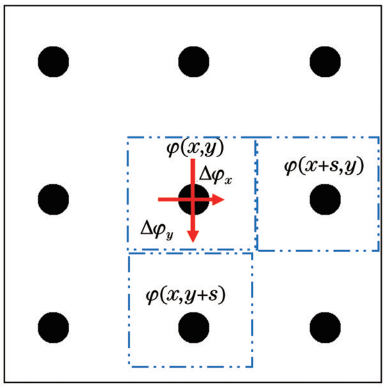

图1　Southwell模型波前重构

Fig. 1　Wavefront reconstruction based on Southwell model

$$\begin{cases}\dfrac{\Delta\varphi_x(x,y)+\Delta\varphi_x(x,y+s)}{2}=\dfrac{(\varphi_{i,j+1}-\varphi_{i,j})}{s}, & i\in(1,N),\ j\in(1,N-1)\\ \dfrac{\Delta\varphi_y(x,y)+\Delta\varphi_y(x+s,y)}{2}=\dfrac{(\varphi_{i+1,j}-\varphi_{i,j})}{s}, & i\in(1,N-1),\ j\in(1,N)\end{cases},\tag{4}$$

式中：s为剪切量；$\Delta\varphi_x$和$\Delta\varphi_y$分别为x方向和y方向的差分波前。

沿着剪切方向对差分波前进行迭代积分求解，可将式(4)改写成

$$\begin{cases}\varphi_{i,j+1}=\dfrac{s}{2}\cdot\left[\Delta\varphi_x(x,y)+\Delta\varphi_x(x,y+s)\right]+\varphi_{i,j}, & i\in(1,N),\ j\in(1,N-1)\\ \varphi_{i+1,j}=\dfrac{s}{2}\cdot\left[\Delta\varphi_y(x,y)+\Delta\varphi_y(x+s,y)\right]+\varphi_{i,j}, & i\in(1,N-1),\ j\in(1,N)\end{cases}。\tag{5}$$

在干涉图不存在噪声且满足采样定理的情况下，以差分相位中的像素点(i,j)为初始点，沿着剪切方向（任意路径）按照式(5)计算每个像素点上的相位，最终遍历所有差分相位点即可求得待测波前相位。根据高斯定理，积分结果与积分路径无关，因此积分路径的选取不影响波前重构的结果。但在实际的光学测量中，四波横向剪切干涉图由于各种原因会存在噪声误差、无效区域、对比度低、被测轮廓跳变或者条纹欠采样等问题，导致差分相位具有噪声点，因此将式(5)改写成

$$\begin{cases}\varphi_{i,j+1}=\dfrac{s}{2}\cdot\left[\Delta\varphi_x(x,y)+\Delta\varphi_x(x,y+s)+\varepsilon_x\right]+\varphi_{i,j}, & i\in(1,N),\ j\in(1,N-1)\\ \varphi_{i+1,j}=\dfrac{s}{2}\cdot\left[\Delta\varphi_y(x,y)+\Delta\varphi_y(x+s,y)+\varepsilon_y\right]+\varphi_{i,j}, & i\in(1,N-1),\ j\in(1,N)\end{cases},\tag{6}$$

式中：ε_x和ε_y分别为x和y方向的噪声。

若直接沿着剪切方向积分，就会导致噪声点ε_x和ε_y沿着剪切方向叠加累积，影响波前重构精度。

2.2 路径导引的波前重构

为了解决传统区域法中噪声沿积分方向传播从而影响波前重构精度的问题，笔者采用差分相位导数偏差模型统计差分相位的变化特征，以识别噪声误差，进而生成规避噪声误差的积分路径，如图2(b)所示。本文采用的差分相位导数偏差模型定义为

$$q_{m,n}=\frac{\sqrt{\sum_{i=m-k/2}^{m+k/2}\sum_{j=n-k/2}^{n+k/2}\left(\Delta\varphi_{i,j}^{x}-\Delta\varphi_{m,n}^{\bar{x}}\right)^2}+\sqrt{\sum_{i=m-k/2}^{m+k/2}\sum_{j=n-k/2}^{n+k/2}\left(\Delta\varphi_{i,j}^{y}-\Delta\varphi_{m,n}^{\bar{y}}\right)^2}}{k\times k},\tag{7}$$

式中：$\Delta\varphi_{i,j}^{x}$和$\Delta\varphi_{i,j}^{y}$为差分相位；$\Delta\varphi_{m,n}^{\bar{x}}$和$\Delta\varphi_{m,n}^{\bar{y}}$为差分相位的平均值。由式(7)可知，若在计算窗$k\times k$内存在噪声点，则此噪声点处的评价值相比周围相位点会有一个突变，根据评价值突变判定此点为噪声点。点(m,n)处的评价值$q_{m,n}$越小，则此处对应的差分相位的信噪比越高，该点附近的波前相位相对越平滑。

根据式(7)求出差分相位的评价值，依据评价值的大小建立待测相位队列，如图 2(b)～(d)所示；然后将待测相位队列中差分相位点的顺序作为积分路径，指引式(6)进行波前重构积分，即可规避噪声点的传播与累积，如图 2(e)所示。

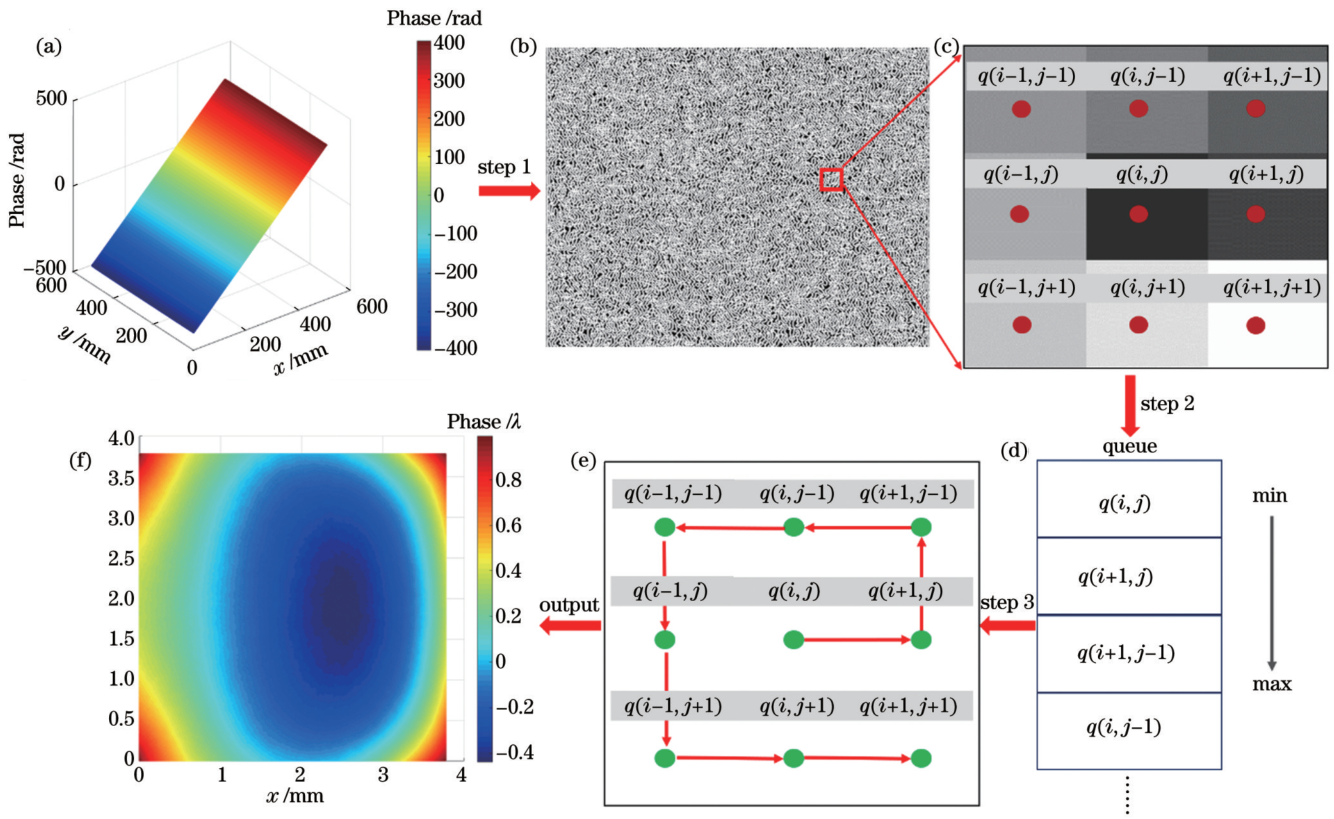

图2 波前重构原理图。(a)差分相位；(b)差分相位导数偏差评价图；(c)局部评价图；(d)波前重构积分队列；(e)波前重构积分；(f)波前重构结果

Fig. 2 Schematics of wavefront reconstruction. (a) Differential phase; (b) differential phase derivative deviation evaluation map; (c) partial evaluation map; (d) wavefront reconstruction integral queue; (e) wavefront reconstruction integral; (f) wavefront reconstruction result

3 算 法

基于积分路径导引的重构算法流程如图 3 所示，主要分为以下步骤：1)截取有效计算范围；2)对计算范围内的干涉图进行快速傅里叶变换(FFT)并提取正交方向的±1级频谱信息；3)对±1级频谱进行傅里叶逆变换(IFFT)；4)对提取出来的包裹差分相位进行相位解包裹；5)通过式(7)分别计算x方向和y方向上的差分相位导数偏差评价图，并建立待测相位队列；6)将评价图作为积分路径，利用式(6)对待测相位进行波前重构积分；7)删除队列中已重构的相位点，并将下一个待测点推入队列；8)判断队列是否为空；9)完成波前重构。具体算法步骤如下所述：

Step1：输入四波横向剪切干涉图I_0。

Step2：截取干涉图的计算区域$M\times N$。

Step3：对计算区域进行 FFT 得到频谱，并利用滤波窗口提取出正交方向的±1级频谱，即

$$\mathrm{Wrap}(\widetilde{\Delta\varphi_x})=W_x\times\mathrm{FFT}(I_{M\times N}),\tag{8}$$

$$\mathrm{Wrap}(\widetilde{\Delta\varphi_y})=W_y\times\mathrm{FFT}(I_{M\times N}),\tag{9}$$

其中，

$$W_{x,y}=\frac{1}{2\pi\sigma^2}\exp\left(-\frac{x^2+y^2}{2\sigma^2}\right)\times\left[1+\frac{x^2}{2\sigma^2}+\frac{1}{2}\times\left(\frac{x^2}{2\sigma^2}\right)^2+\frac{1}{6}\times\left(\frac{x^2}{2\sigma^2}\right)^3\right]\times\left[1+\frac{y^2}{2\sigma^2}+\frac{1}{2}\times\left(\frac{y^2}{2\sigma^2}\right)^2+\frac{1}{6}\times\left(\frac{y^2}{2\sigma^2}\right)^3\right],\tag{10}$$

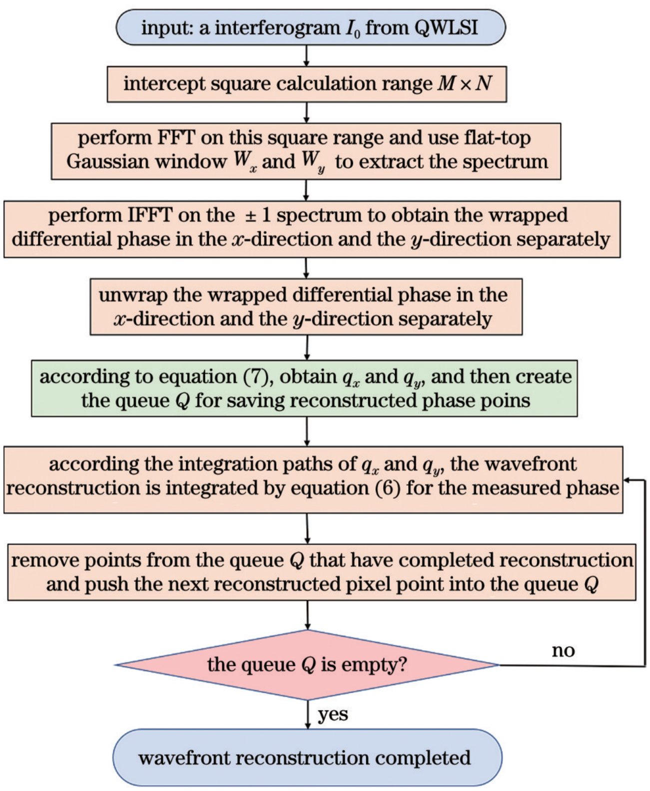

图 3 基于路径导引的波前重构算法流程图

Fig. 3 Flowchart of path-guided wavefront reconstruction algorithm

式中，$\widetilde{\Delta\varphi_x}$和$\widetilde{\Delta\varphi_y}$分别为$x$方向和$y$方向的+1级频谱，Wrap为相位包裹算子，$W$为平顶高斯滤波窗，$\sigma$为平顶高斯函数的标准方差。

Step4：对式(8)、(9)进行傅里叶逆变换，得到x方向和y方向的包裹差分相位，即

$$\mathrm{Wrap}(\Delta\varphi_x)=\mathrm{IFFT}\left[\mathrm{Wrap}(\widetilde{\Delta\varphi_x})\right],\tag{11}$$

$$\mathrm{Wrap}(\Delta\varphi_y)=\mathrm{IFFT}\left[\mathrm{Wrap}(\widetilde{\Delta\varphi_y})\right]。\tag{12}$$

Step5：利用基于离散余弦变换的最小二乘法对式(11)、(12)进行相位解包裹，得到x方向和y方向的差分相位，即

$$\Delta\varphi_x=\mathrm{Unwrap}\left[\mathrm{Wrap}(\Delta\varphi_x)\right],\tag{13}$$

$$\Delta\varphi_y=\mathrm{Unwrap}\left[\mathrm{Wrap}(\Delta\varphi_y)\right],\tag{14}$$

式中，Unwrap为解包裹算子。

Step6：针对解包裹后的差分相位$\Delta\varphi_x$和$\Delta\varphi_y$，利用式(7)分别求出x方向和y方向的差分相位导数偏差评价图q_x和q_y，并建立队列Q来储存待重构相位点。

Step7：将评价图q_x和q_y作为积分路径，利用式(6)所示Southwell波前重构积分模型对待测相位进行重构积分。以评价图中评价值最小的点作为积分起始点，并将起始点及周围的待测点推入队列Q，从评价值低处向评价值高处进行波前重构积分。

Step8：删除队列Q中已重构的像素点，并将下个待重构像素点推入队列Q。

Step9：若队列Q为空，完成重构，否则，跳转至Step7进行下个相位点的重构。

Step10：待测波前重构完成。

4 仿真分析

为了验证所提方法的有效性，按如下设定仿真参数：

1) 对于光场，设定其波长λ=530 nm，相位是振幅分布均匀的正弦信号，大小归一化在[$-\lambda$,λ]内，孔径形状为圆形，计算矩阵大小为512×512，如图4(a)所示。

2) 对于探测器，设定CCD像元尺寸为l=7.4 μm，CCD采样点数为1024×1024，探测器测得的四波横向剪切干涉图如图4(b)所示。

3) 设定添加的噪声是均值为0、均方差为0.96的高斯白噪声，如图5(a)所示。

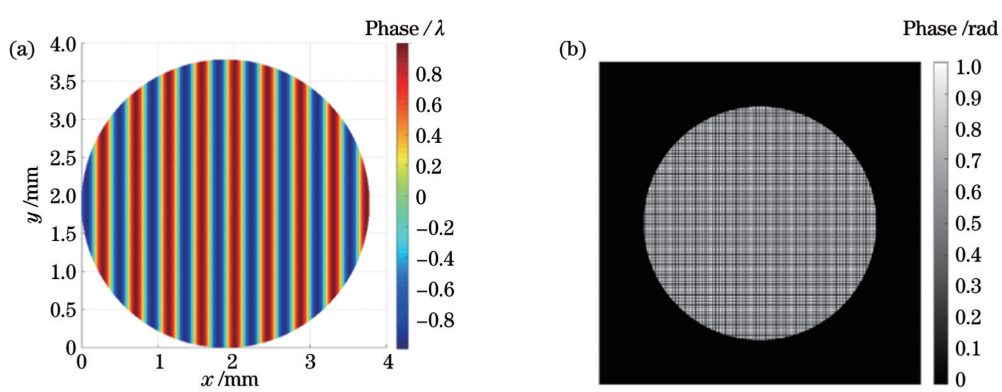

图 4 理论仿真。(a)理论的入射光场波前；(b)CCD探测的干涉图

Fig. 4 Theoretical simulation. (a) Theoretical wavefront of incident light field; (b) interferogram detected by CCD

将不同信噪比的高斯白噪声分别添加至理论仿真的四波横向剪切干涉图中，并将其与无积分路径导引区域法的波前重构结果进行对比。由图6(a)～(e)可以看出无积分路径导引区域法将噪声点沿x和y方向进行传播与累积，形成了“噪声线”。如图6(f)～(j)所示，本文所提方法有效阻止了噪声点沿剪切方向的传

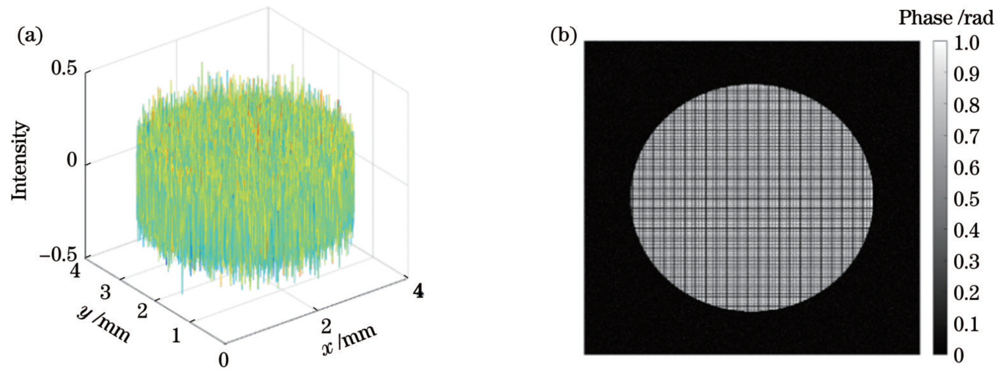

图 5　理论仿真。(a)高斯白噪声；(b)CCD探测的干涉图

Fig. 5　Theoretical simulation. (a) Gaussian noise; (b) interferogram detected by CCD

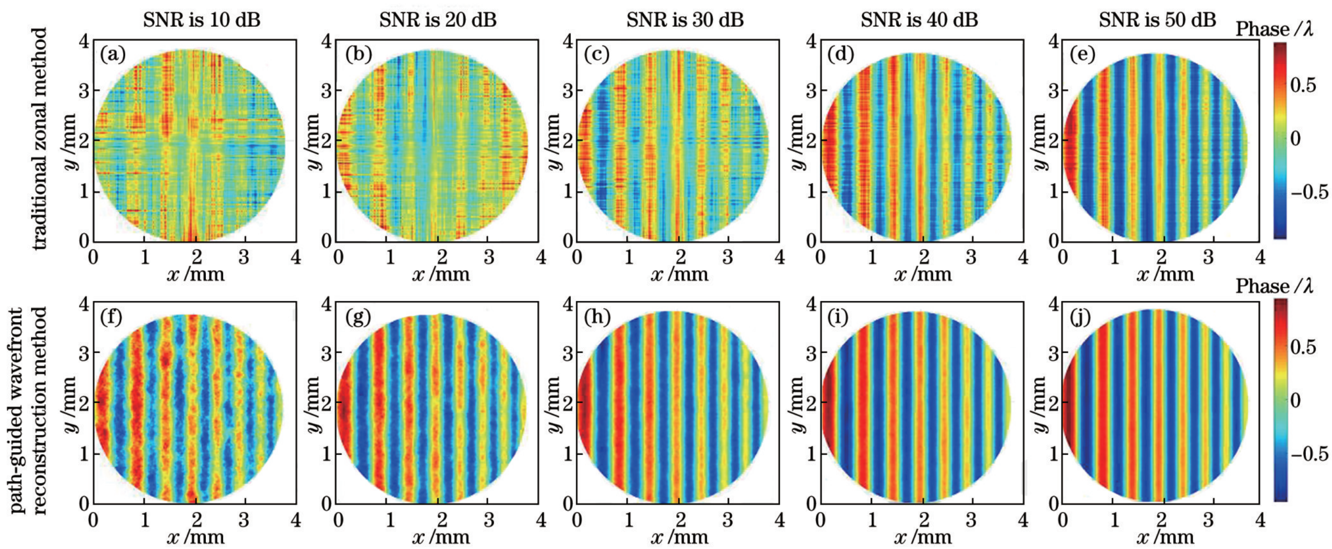

图 6　噪声环境下无积分路径导引区域法与基于积分路径导引的重构方法的仿真结果。(a)～(e)无积分路径导引区域法的波前重构结果；(f)～(j)基于积分路径导引的波前重构结果

Fig. 6　Simulation results of the zonal method without integral-path guidance and the integral-path-guided reconstruction method in noisy environment. (a)–(e) Wavefront reconstruction of the zonal method without integral-path guidance; (f)–(j) integral-path-guided wavefront reconstruction

播，提高了波前重构精度，与2.2节所述积分路径导引的波前重构原理一致。

在不同的信噪比（SNR）下，笔者计算了所提方法与理论波前残差的RMS以及无积分路径导引区域法的结果与理论波前残差的RMS，如图7所示。随着信噪比由10 dB增大至50 dB，无积分路径导引区域法的重构波前与理论波前残差的RMS由0.0152λ降至0.0094λ，而本文所提方法重构波前与理论波前残差的RMS由0.0139λ降低至0.0041λ，且所提方法的波前重构结果与理论值残差的RMS偏差相比无积分路径导引波前重构结果与理论值残差的RMS偏差最大降低了55.6%。因此，所提方法相较于无积分路径区域法具有更好的噪声鲁棒性，且与图6所示结果具有一致性。

在不同信噪比噪声环境下，差分相位导数偏差模型计算窗k值会影响评价图的质量，进而影响波前重构精度。通过理论仿真得到了k取不同值时波前重构

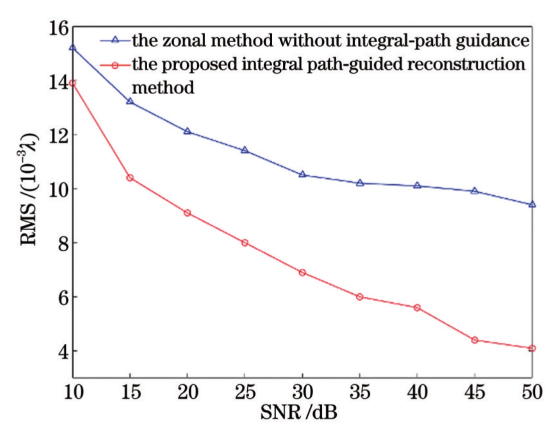

图 7　积分路径导引重构方法的结果、无积分路径导引区域法的结果与理论波前残差的RMS

Fig. 7　RMS of the residuals between the integral-path-guided reconstruction results and the theoretical wavefront, as well as RMS of the residuals between the zonal wavefront reconstruction results without integral-path guidance and the theoretical wavefront

残差的RMS，如图8所示。波前重构残差的RMS随着信噪比的增加而降低；当信噪比为40 dB～50 dB时，波前重构残差的RMS最大，为0.0081λ(k=9)；当信噪比为10 dB～35 dB时，k取3对应的波前重构残差的RMS最小。

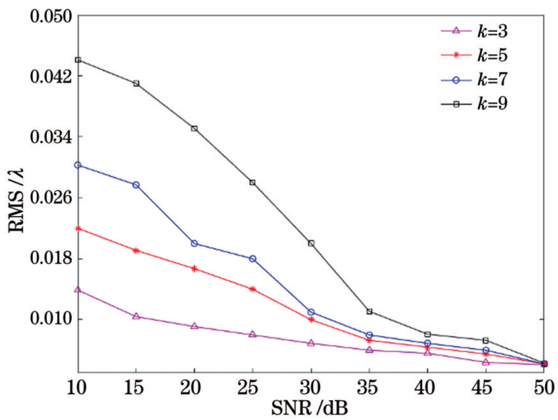

图8　k值对波前重构残差的影响

Fig. 8　Influence of k value on wavefront reconstruction residual

5　实验与分析

5.1　实验装置

实验光路如图9所示。光纤点源经准直扩束镜准直为平行光，之后经格兰棱镜调整为水平偏振态后入射至空间光调制器(SLM)，再经空间光调制器调制后入射至QWLSI。利用纯相位型空间光调制器对平面波进行调制，产生具有随机相位的波前，然后利用QWLSI进行测量，最后通过所提方法重构待测波前，验证所提方法的有效性。

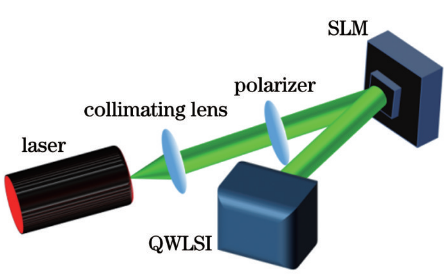

图9　实验光路示意图

Fig. 9　Schematic of the experimental optical path

搭建的实验装置如图10所示。该装置主要由光纤激光器、准直扩束系统、格兰棱镜、纯相位液晶空间调制器以及QWLSI组成。实验装置参数如下：1)光纤激光器输出波长λ=530 nm；2)准直扩束系统的焦距为100 mm，口径为20 mm；3)格兰棱镜通光口径为15 mm；4)纯相位液晶空间光调制器的分辨率为1920×1200，像元大小为8 μm；5)QWLSI中光栅材料的折射率为1.457，台阶高度为579.89 nm，振幅光栅周期为0.0296 mm，光栅一个周期内透光部分的边长为0.0197 mm。

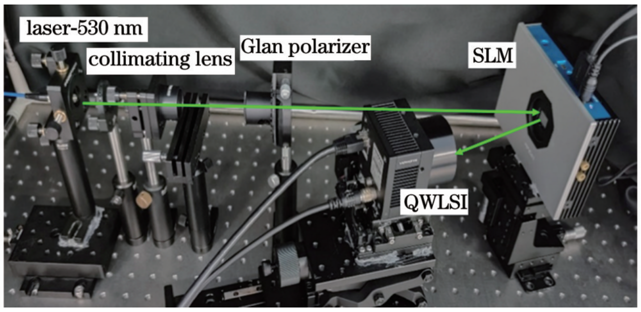

图10　实验装置

Fig. 10　Experimental device

5.2　实验结果与分析

搭载在纯相位空间光调制器上的随机相位如图11所示，每个方格占空间相位调制器4个像素。QWLSI采集的干涉图如图12(a)所示，x方向和y方向的差分相位导数偏差评价图q_x和q_y分别为图12(b)和图12(c)，图13(a)和图13(b)分别为无积分路径导引区域法和本文所提方法对随机相位的部分区域波前重构的结果。

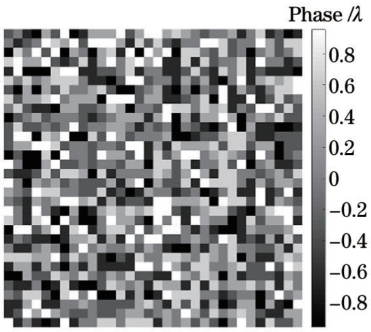

图11　空间相位调制器加载的理论相位

Fig. 11　Theoretical phase loaded by SLM

在光场传播过程和数据处理阶段，由于相机光瞳大小和计算范围的限制，重构出的相位图是理论相位图的一部分区域，如图13所示。在相同的计算区域内，所提方法重构波前峰谷值(PV值)为0.7283λ，无积分路径导引区域法重构波前PV值为2.966λ，前者与理论波前PV值的偏差相较于后者与理论波前PV值的偏差减小了1.6943λ，且前者与理论波前残差的RMS相比后者与理论波前残差的RMS降低了39.7%。无积分路径导引区域法重构波前有严重的“噪声线”，甚至无法重构出随机相位信息，而所提方法可以有效地重构出空间光调制器上加载的随机信息。可见，在重构具有边界和噪声的随机相位时，所提方法能够更有效地处理噪声和边界带来的问题。

6　结　　论

本文提出了一种基于积分路径导引的四波横向剪切干涉波前重构方法。首先分析了噪声环境下无积分路径导引区域法重构波前存在噪声沿积分方向传播与

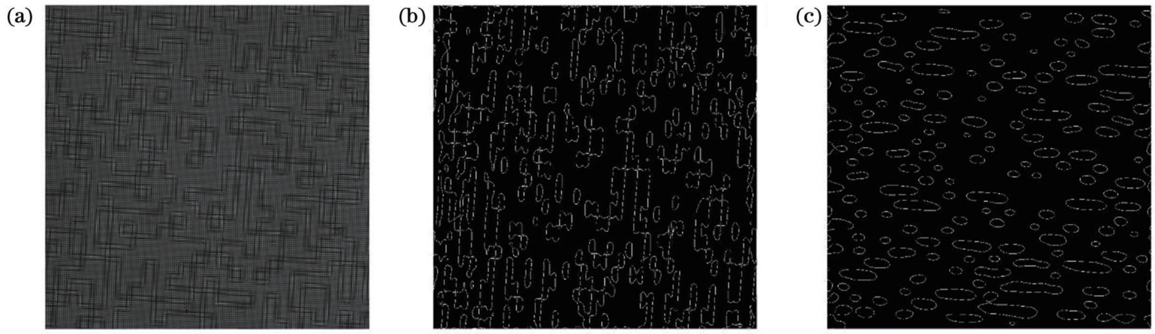

图 12　CCD 采集的干涉图和正交方向的差分相位导数偏差评价图。(a)CCD 采集的四波横向剪切干涉图；(b)x 方向的差分相位导数偏差评价图；(c)y 方向的差分相位导数偏差评价图

Fig. 12　Interferogram acquired by CCD and derivative deviation evaluation diagrams of the differential phase in orthogonal direction. (a) Quadri-wave lateral shearing interferogram acquired by CCD; (b) derivative deviation evaluation diagram of the differential phase in the x direction; (c) derivative deviation evaluation diagram of the differential phase in the y direction.

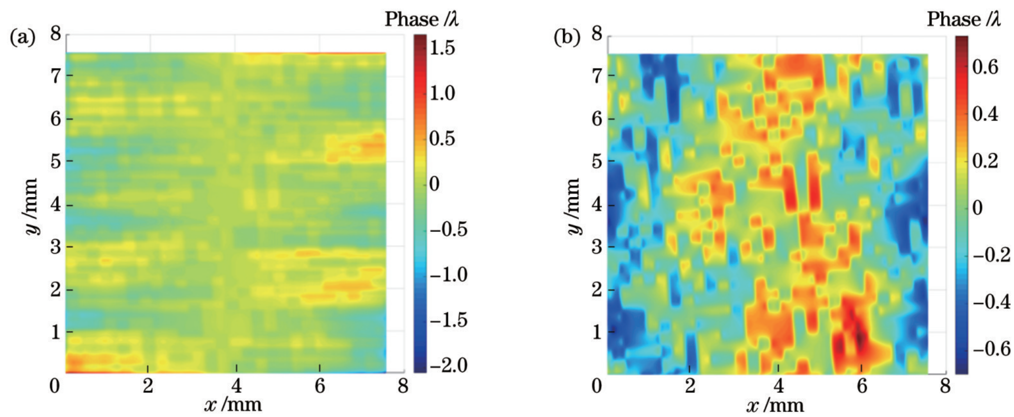

图 13　波前重构结果。(a)无积分路径导引区域法波前重构结果；(b)积分路径导引的波前重构结果

Fig. 13　Wavefront reconstruction results. (a) Zonal wavefront reconstruction without integral-path guidance; (b) integral-path-guided wavefront reconstruction

累积的问题，然后在此基础上建立了基于差分相位导数的偏差模型，用于对差分相位重构进行排序，阻止噪声的传播，消除“噪声线”。同时，给出了基于积分路径导引的波前重构算法的流程。正弦波前的理论仿真结果显示，当添加的高斯白噪声的信噪比由 10 dB 增大到 50 dB 时，无积分路径导引区域法重构波前与理论波前残差的 RMS 由 0.0152λ 降低至 0.0094λ，而所提方法重构波前与理论波前残差的 RMS 由 0.0139λ 降至 0.0041λ，且所提方法重构波前与理论波前残差的 RMS 相比无积分路径导引区域法重构波前与理论波前残差的 RMS 最大降低了 55.6%。

设计并搭建了基于纯相位型液晶空间光调制器的实验验证装置。分别采用所提方法和无积分路径导引区域法重构随机相位，所提方法重构波前 PV 值为 0.7283λ，无积分路径导引区域法重构波前 PV 值为 2.966λ，所提方法波前重构结果与理论波前 PV 值的偏差相较于无积分路径导引区域法波前重构结果与理论波前 PV 值的偏差减小了 1.6943λ，且所提方法重构波前与理论残差的 RMS 相较于无积分路径导引区域法重构波前与理论残差的 RMS 降低了 39.7%。仿真和实验结果表明，在噪声影响下，所提积分路径导引波前重构算法的精度优于无积分路径导引区域法的波前重构精度，且具有更高的鲁棒性。因此，在噪声环境下，本文所提重构方法有望为四波横向剪切干涉测量技术提供一种新的高精度波前重构方法。

参　考　文　献

[1] Velghe S, Primot J, Guérineau N, et al. Wave-front reconstruction from multidirectional phase derivatives generated by multilateral shearing interferometers[J]. Optics Letters, 2005, 30(3): 245-247.

[2] 岳秀梅, 杨甬英, 凌曈, 等. 可用于四波横向剪切干涉波前检测的随机编码混合光栅设计[J]. 中国激光, 2015, 42(10): 1008006.

[3] Li P, Tang F, Wang X Z. Comparison of processing speed of typical wavefront reconstruction methods for lateral shearing interferometry[J]. Applied Optics, 2021, 60(2): 312-325.

[4] Ling T, Yang Y Y, Yue X M, et al. Common-path and compact wavefront diagnosis system based on cross grating lateral shearing interferometer[J]. Applied Optics, 2014, 53(30): 7144-7152.

[5] Ling T, Yang Y Y, Liu D, et al. General measurement of optical system aberrations with a continuously variable lateral shear ratio by a randomly encoded hybrid grating[J]. Applied Optics, 2015, 54(30): 8913-8920.

[6] Bon P, Maucort G, Wattellier B, et al. Quadriwave lateral shearing interferometry for quantitative phase microscopy of living

cells[J]. Optics Express, 2009, 17(15): 13080-13094.

[7] Bon P, Wattellier B, Monneret S. Modeling quantitative phase image formation under tilted illuminations[J]. Optics Letters, 2012, 37(10): 1718-1720.

[8] Wang J Y, You W, Jiao Y H, et al. Quadriwave gradient light inteference microscopy for lable-free thick sample imaging[J]. Optics Express, 2021, 29(25): 41719-41730.

[9] Baffou G. Quantitative phase microscopy using quadriwave lateral shearing interferometry (QLSI): principle, terminology, algorithm and grating shadow description[J]. Journal of Physics D: Applied Physics, 2021, 54(29): 294002.

[10] Dai F Z, Tang F, Wang X Z, et al. Modal wavefront reconstruction based on Zernike polynomials for lateral shearing interferometry: comparisons of existing algorithms[J]. Applied Optics, 2012, 51(21): 5028-5037.

[11] Bon P, Aknoun S, Monneret S, et al. Enhanced 3D spatial resolution in quantitative phase microscopy using spatially incoherent illumination[J]. Optics Express, 2014, 22(7): 8654-8671.

[12] Tian X, Itoh M, Yatagai T. Simple algorithm for large-grid phase reconstruction of lateral-shearing interferometry[J]. Applied Optics, 1995, 34(31): 7213-7220.

[13] Liu K, Wang J, Wang H, et al. Wavefront reconstruction for multi-lateral shearing interferometry using difference Zernike polynomials fitting[J]. Optics and Lasers in Engineering, 2018, 106: 75-81.

[14] Gu N T, Huang L H, Yang Z P, et al. Modal wavefront reconstruction for radial shearing interferometer with lateral shear [J]. Optics Letters, 2011, 36(18): 3693-3695.

[15] Li J, Tang F, Wang X Z, et al. Wavefront reconstruction for lateral shearing interferometry based on difference polynomial fitting[J]. Journal of Optics, 2015, 17(6): 065401.

[16] Guo Y F, Chen H, Xu J, et al. Two-dimensional wavefront reconstruction from lateral multi-shear interferograms[J]. Optics Express, 2012, 20(14): 15723-15733.

[17] 曾新, 梁佩莹, 丁剑平. 大剪切量干涉的二维波前重建[J]. 中国激光, 2005, 32(6): 782-786.
Zeng X, Liang P Y, Ding J P. Two-dimensional wavefront reconstruction of shearing interferograms with big shears[J]. Chinese Journal of Lasers, 2005, 32(6): 782-786.

[18] 徐文东, 谢元营, 李锡善. 恢复横向剪切干涉原始波面的新方法[J]. 中国激光, 1999, 26(11): 982-986.
Xu W D, Xie Y Y, Li X S. A new method for recovering the original wave-front in lateral-shearing interferometry[J]. Chinese Journal of Lasers, 1999, 26(11): 982-986.

[19] 赵冬娥, 李诺伦, 马亚云, 等. 基于剪切干涉的双涡旋光干涉图样特性研究[J]. 激光与光电子学进展, 2021, 58(11): 1108001.
Zhao D E, Li N L, Ma Y Y, et al. Characteristics of double-vortex optical interferogram based on shearing interference[J]. Laser & Optoelectronics Progress, 2021, 58(11): 1108001.

[20] 宋静威, 李常伟, 张思炯. 基于离焦型夏克-哈特曼传感器的定量相位成像技术[J]. 光学学报, 2021, 41(9): 0911002.

[21] Yin Z Q. Exact wavefront recovery with tilt from lateral shear interferograms[J]. Applied Optics, 2009, 48(14): 2760-2766.

[22] Dai F Z, Tang F, Wang X Z, et al. High spatial resolution zonal wavefront reconstruction with improved initial value determination scheme for lateral shearing interferometry[J]. Applied Optics, 2013, 52(17): 3946-3956.

[23] 何煦, 袁理. 基于子孔径斜率离散采样的波前重构[J]. 光学 精密工程, 2016, 24(1): 20-29.
He X, Yuan L. Wavefront reconstruction based on discrete sampling of sub-aperture slope[J]. Optics and Precision Engineering, 2016, 24(1): 20-29.

[24] Hudgin R H. Wave-front reconstruction for compensated imaging [J]. Journal of the Optical Society of America, 1977, 67(3): 375-378.

[25] Fried D L. Least-square fitting a wave-front distortion estimate to an array of phase-difference measurements[J]. Journal of the Optical Society of America, 1977, 67(3): 370-375.

[26] Southwell W H. Wave-front estimation from wave-front slope measurements[J]. Journal of the Optical Society of America, 1980, 70(8): 998-1006.

[27] Nomura T, Okuda S, Kamiya K, et al. Improved Saunders method for the analysis of lateral shearing interferograms[J]. Applied Optics, 2002, 41(10): 1954-1961.

[28] Servin M, Malacara D, Marroquin J L. Wave-front recovery from two orthogonal sheared interferograms[J]. Applied Optics, 1996, 35(22): 4343-4348.

[29] Elster C. Exact two-dimensional wave-front reconstruction from lateral shearing interferograms with large shears[J]. Applied Optics, 2000, 39(29): 5353-5359.

[30] Liu J N, Meng J, Lyu J H, et al. Fast reconstruction technology of a laser beam spatial transmission characteristic curve[J]. Applied Optics, 2022, 61(5): 1177-1182.

[31] Malacara D. Twyman-green interferometer[M]//Optical shop testing. Hoboken: John Wiley & Sons, Inc., 2007: 46-96.

Quadri-Wave Lateral Shearing Interference Wavefront Reconstruction Based on Path Guidance

Min Xingzhi[1,2,3], Duan Yaxuan[1,3*], Wang Zhengzhou[1,3], Chen Xiaoyi[1,3], Tang Zhiyuan[1,3], Wang Pu[1,3], Fan Yao[1,3]

[1] *Advanced Optical Instrument Research Department, Xi'an Institute of Optics and Precision Mechanics, Chinese Academy of Sciences, Xi'an* 710119, *Shaanxi, China*;

[2] *University of Chinese Academy of Science, Beijing* 100049, *China*;

[3] *Xi'an Key Laboratory of High Power Laser Measurement Technology and Instrumentation, Xi'an* 710119, *Shaanxi, China*

Abstract

Objective The accuracy of a quadri-wave lateral shearing interferometer is directly affected by the accuracy of the wavefront reconstruction. Traditional wavefront-reconstruction methods include modal and zonal methods. The modal method expands the wavefront into a set of primary functions to be measured, then fits the coefficients corresponding to the primary functions to reconstruct the measured wavefront. The zonal method discretizes the measured wavefront to establish a mapping relationship between the measured and differential wavefronts for reconstruction. Alternatively, the wavefront can be reconstructed by direct integration in the shearing direction. However, the modal method always uses finite terms to fit the measured wavefront, which directly ignores high-frequency information, reducing the estimated accuracy of the quadri-wave lateral shearing interferometer. The zonal method has a high spatial resolution, but the noise error accumulates along the integrated path during the reconstruction process, forming noise lines, thus, affecting the accuracy of the reconstructed wavefront. To solve this problem, a quadri-wave lateral shearing interferometric wavefront reconstruction method is proposed based on path guidance, which has both high accuracy and spatial resolution.

Methods In this study, a theoretical analysis of the drawbacks of noise error accumulation in wavefront reconstruction using the zonal method without integral-path guidance under noisy environments is carried out. An integral-path evaluation-map model is established based on the deviation of differential phase derivatives, and a flowchart of the wavefront reconstruction algorithm is provided based on integral-path guidance. The proposed method consists of two steps. First, the evaluation model of the differential-phase-derivative deviation is used to count the variational characteristics of the differential phase, identify the noise error, and generate an integral path to avoid noise error. Second, the generated path is used to guide the wavefront reconstruction integral of the Southwell model. Using theoretical simulations, the proposed method could effectively prevent the propagation and accumulation of noise errors compared to the zonal method without integral-path guidance under noisy environments for different signal-to-noise ratios (SNRs). In addition, a verification device having a pure-phase liquid-crystal spatial light modulator (SLM) was set up to experimentally verify the effectiveness of the proposed method. The experimental results of the proposed method were also compared with those of the zonal method without integral-path guidance.

Results and Discussions In the simulation, interferograms with a sinusoidal phase distribution are generated (Fig. 4). When the SNR increases from 10 dB to 50 dB, the root-mean-square (RMS) between the wavefront reconstructed by the zonal method without integral-path guidance and the theoretical wavefront decreases from 0.0152λ to 0.0094λ. However, the RMS between the wavefront reconstructed by the proposed method and the theoretical wavefront decreases from 0.0139λ to 0.0041λ. Moreover, the proposed method reduces the RMS of the reconstructed and theoretical wavefronts by a maximum of 55.6% compared to the zonal method without integral-path guidance (Fig. 7). Thus, the proposed method is more robust than the zonal method without integral-path guidance under the Gaussian noise environment with different SNRs (Fig. 6). In the experiment, we measure the random phase generated by the spatial light modulator using the proposed method and zonal method without integral-path guidance (Fig. 10). The results show that the PV value (peak-valley value) of the wavefront reconstructed by the proposed method is 0.7283λ, whereas that of the wavefront reconstructed by the zonal method without integral-path guidance is 2.966λ. The deviation between the PV value of the wavefront reconstructed by the proposed method and that of the theoretical wavefront is 1.6943λ, which is less than the deviation between the wavefront PV value reconstructed by the zonal method without integral-path guidance and the theoretical wavefront PV value (Fig. 13). In addition, the RMS between the wavefront reconstructed by the proposed method and the theoretical wavefront is reduced by 39.7% compared with the RMS between the wavefront reconstructed by the zonal method without integral-path guidance and the theoretical wavefront. In addition, the zonal method without integral-path guidance is used to reconstruct the wavefront, which propagates and accumulates noise points along the shearing direction by forming noise lines. However, the proposed method prevents the propagation of noise points and improves wavefront reconstruction accuracy.

Conclusions This paper proposes a quadri-wave lateral shearing interference wavefront reconstruction method based on integral-path guidance. The effectiveness of the proposed method is verified through theoretical simulations and experiments. The theoretical simulation results show that the proposed method prevents the propagation of noise errors and improves the wavefront reconstruction accuracy compared to the zonal method without integral-path guidance under noisy environments with different SNRs. The RMS between the reconstructed wavefronts of the proposed method and the theoretical wavefront is smaller than that between the zonal method without integral-path guidance and the theoretical wavefront under the same conditions. Moreover, the experimental results show that the proposed method can effectively prevent the propagation and accumulation of differential phase noise points when measuring the random phase generated by the pure-phase liquid crystal spatial light modulator and reconstructing the wavefront of the random phase. However, the wavefront of the random phase reconstructed using the zonal method without integral-path guidance cannot be accurately reconstructed because of the noise line generated by the accumulation of noise. Therefore, the proposed method has higher accuracy and robustness than the zonal method without integral-path guidance in reconstructing the wavefront in a noisy environment.

Key words measurement; wavefront reconstruction; path-guidance; quadri-wave lateral shearing interference; differential phase